



저작자표시-비영리-변경금지 2.0 대한민국

이용자는 아래의 조건을 따르는 경우에 한하여 자유롭게

- 이 저작물을 복제, 배포, 전송, 전시, 공연 및 방송할 수 있습니다.

다음과 같은 조건을 따라야 합니다:



저작자표시. 귀하는 원저작자를 표시하여야 합니다.



비영리. 귀하는 이 저작물을 영리 목적으로 이용할 수 없습니다.



변경금지. 귀하는 이 저작물을 개작, 변형 또는 가공할 수 없습니다.

- 귀하는, 이 저작물의 재이용이나 배포의 경우, 이 저작물에 적용된 이용허락조건을 명확하게 나타내어야 합니다.
- 저작권자로부터 별도의 허가를 받으면 이러한 조건들은 적용되지 않습니다.

저작권법에 따른 이용자의 권리는 위의 내용에 의하여 영향을 받지 않습니다.

이것은 [이용허락규약\(Legal Code\)](#)을 이해하기 쉽게 요약한 것입니다.

[Disclaimer](#)

**On the performance of short packet
communication-aid NOMA in VLC systems**

A Thesis Submitted in Partial Fulfilment of the Requirements
for the Degree of

MASTER OF SCIENCE

by

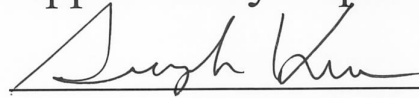
Tran Ngo Giang

**Department of
Electrical, Electronic and Computer Engineering
University of Ulsan**

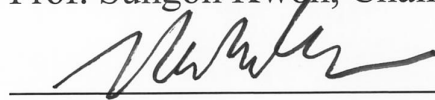
July 2023

**On the performance of short packet
communication-aid NOMA in VLC systems**

Approved by Supervisory Committee:



Prof. Sungoh Kwon, Chair



Prof. Sunghwan Kim, Supervisor



Prof. Hee-Youl Kwak

Department of Electrical, Electronic and Computer Engineering

University of Ulsan, South Korea

Date: July 2023

VITA

Tran Ngo Giang received his Bachelor of Science (B.Sc.) in Electrical Engineering (Advanced Program), Thai Nguyen University of Technology, Vietnam, in 2019. He is currently pursuing the Master's degree with the Department of Electrical, Electronic and Computer Engineering, in University of Ulsan, South Korea. His main research interests are ultra-reliable and low-latency communication, 5G communication, and visible light communication

List of Publications

Journal

1. G. N. Tran and S. Kim, "Performance analysis of short packets in NOMA VLC systems," *IEEE Access*, vol. 10, pp. 6505-6517, Jan. 2022. (This thesis)
2. G. N. Tran and S. Kim, "Performance evaluation of short packet communications in NOMA VLC systems with imperfect CSI," *IEEE Access*, vol. 10, pp. 49871-49793, May 2022.

Conference

1. G. N. Tran, S. Q. Nguyen, M. T. Nguyen, and S. Kim, "Optimal power allocation for non-orthogonal multiple access visible light communications with short packet and imperfect channel information," in *2022 International Conference on Advanced Technologies for Communications (ATC)*, IEEE, Ha Noi, Vietnam, Oct. 2022, pp. 234-238.

ACKNOWLEDGEMENT

First of all, I would like to express my heartfelt gratitude for my advisor Prof. Kim Sunghwan for continuous support for my Master study and related research for his motivation, insightful comments, and knowledge. His invaluable guidance helped me in all the time of research process and writing of this thesis. I could not have imagined having a better advisor and mentor for my Master study.

I would be grateful for departments of electrical, electronic, and computer engineering, Prof. Sungoh Kwon and Prof. Hee-Youl Kwak, for their valuable insights and comments.

I would like to thank all labmates from CITLab, Hieu, Manh, Tuong, Huong, Hoc, and Xiaozhou Lu for discussion, for working together, and all the fun we had.

I would like to acknowledge all my Vietnamese friends in Ulsan, Dr. Tran Ngoc Vinh, Dr. Nguyen Thanh Binh, Dr. Ta Van Khoe, Dr. Tran Huu Phi, Nguyen Tuan Khai, Vo Xuan Thuy, Nguyen Duy Linh, etc. for their wonderful collaboration and supports. All they have given me motivation and comments in both life and research. I am thankful to Vietnamese Student Association at University of Ulsan with enthusiastic support during time of COVID-19 and interesting activities to bring us together.

Beside, I wish to show my appreciation to Prof. Nguyen Tuan Minh, Prof. Nguyen Minh Y, and Dr. Vu Quoc Dong, from Thai Nguyen University of Technology, Vietnam for sharing expertise, giving valuable guidance and encouragement extended to me.

Last but not the least, I would like to express my sincere gratitude to my family for encouragement from Vietnam. I thank to my parents and grandparents's motivation. I would like to thank my brother and sister-in-law for caring my parents. I thank to my cousin, Mrs. Ngo Thu Hien for assistance when I had prepared to study broad. I thank to my darling – a special girl in my heart (HT), for being by my side.

Thank you all very much! Thank University of Ulsan, an active environment for studying. Thank Ulsan – my beloved city! Thank you!

ABSTRACT

On the performance of short packet communication–aid NOMA in VLC systems

by

Tran Ngo Giang

Supervisor: Professor Sunghwan Kim

Submitted in Partial Fulfilment of the Requirements for the Degree of

Master of Science

July 2023

The fifth generation (5G) and beyond are emerging technologies to support high-speed communication, low latency, and massive connectivity. Visible light communication (VLC) is a prospective technology to provide high data rates and low-latency for 5G and beyond. In this thesis, we present a theoretical framework for evaluating the performance of short-packet communication (SPC) in a non-orthogonal multiple access (NOMA) visible light communication (VLC) system. Our proposed system involves one light-emitting diode (LED) transmitting data to two single-photodiode users. To analyze the system performance, we approximate the block error rate (BLER) by using the Gaussian-Chebyshev quadrature method and derive expressions for reliability, throughput, and latency. Additionally, we optimize power allocation coefficients and transmission rates to maximize the sum throughput of the SPC-NOMA VLC system. Our numerical results show that our proposed system meets the strict requirements of ultra-reliable and low latency communication (URLLC) at a signal-to-noise ratio (SNR) greater than 130 dB. Moreover, the SPC-NOMA VLC system exhibits superior performance compared to SPC-orthogonal multiple access

(OMA) VLC systems in terms of reliability, latency, and throughput. We also investigate the impact of block length, power allocation coefficients, transmission rates, and LED semi-angle. Moreover, numerical search method is utilized to find optimal solution for maximizing the system throughput.

Contents

List of Figures	x
List of Tables	xii
1 Introduction	1
1.1 Visible light communication	1
1.2 Related works and motivation	3
1.3 Contribution	6
1.4 Thesis Organization	7
2 SPC-NOMA VLC system	8
2.1 Preliminary	8
2.1.1 System model	8

2.1.2	Short packet communication (SPC)	10
2.1.3	NOMA in VLC systems	12
2.1.4	OMA in VLC systems	15
2.1.5	VLC channel and distribution of received signal-to-noise ratio	15
2.2	Performance analysis	18
2.2.1	Average BLER in VLC systems	18
2.2.2	SPC in NOMA VLC systems	20
2.2.3	SPC in OMA VLC systems	22
2.3	Numerical results	23
3	Optimal sum throughput design	31
3.1	Optimization problem	31
3.2	Optimal design	32
3.3	Results	35
4	Conclusions	38
A	Proof of proposition 3.2.1	39
B	Proof of proposition 3.2.2	41

C Proof of Lemma 3.2.4	42
D Proof of Lemma 3.2.5	44
Bibliography	46

List of Figures

2.1	Illustration of the SPC-LPC in NOMA and OMA VLC system. (a) Proposed overall system model with VLC. (b) NOMA and OMA transmission. (c) SPC versus LPC.	9
2.2	Principle of the two-user NOMA and VLC systems.	13
2.3	Average BLER comparison between NOMA versus OMA using SPC with different power allocation strategies.	24
2.4	SPC and LPC for NOMA VLC.	26
2.5	The reliability of the SPC in NOMA and OMA VLC system.	27
2.6	Latency comparison between NOMA versus OMA using SPC.	28
2.7	Throughput of SPC for NOMA and OMA.	29
2.8	The sum throughput for different values of semi-angles at different SNR.	30
3.1	Sum throughput as the function of the power allocation for U_2 at $\gamma_{Tx} = 126$ dB, $R_1 = 0.4$, and $R_2 = 0.35$	34

3.2	Sum throughput for the near user and the maximum throughput point	
	$(R_2, R_1, \bar{T}) = (1.2, 0.5, 1.17), \gamma_{\text{Tx}} = 126$ dB.	35

List of Tables

2.1 SIMULATION PARAMETERS 23

Notations and Abbreviations

5G	Fifth-generation
BLER	Block error rate
CSI	Channel state information
DC	Direct current
IM/DD	Intensity modulation and direct detection
LED	Light-emitting diode
LPC	Long packet communication
NOMA	Non-orthogonal multiple access
OMA	Orthogonal multiple access
RF	Radio frequency
SIC	Successive interference cancellation
SNR	Signal-to-noise ratio
SPC	Short packet communication
URLLC	Ultra-Reliable Low Latency Communication
VLC	Visible light communication

Chapter 1

Introduction

1.1 Visible light communication

The exponential increase of mobile devices with high-speed demand of current wireless service causes to congestion in traditional radio frequency (RF) communication systems [1]. To deal with the problem of RF systems, new communication technologies have been developed. Among the emerging communication technologies visible light communication (VLC) has the potential to revolutionize wireless communication systems. VLC frequency spectrum is in the range of terahertz (400 THz to 800 THz) [1]. This is approximately 10,000 times larger than that of RF systems.

VLC systems utilize visible light, specifically light-emitting diodes (LEDs), as a medium for transmitting data instead of traditional radio frequencies. The basic components of a VLC system are an LED as the transmitter and a photodiode (PD) as receiver [2]. LED is modulated to encode the data to be transmitted. The encoded

data is modulated to the corresponding intensity or frequency of the light emitted from the LED. The data can be encoded using various modulation techniques, such as on-off keying (OOK), pulse position modulation (PPM), or frequency shift keying (FSK). A photodetector converts the modulated light signal into an electrical signal. The receiver must be synchronized with the transmitter to correctly decode the transmitted data. VLC systems can operate in two modes: line-of-sight (LOS) and diffuse. In the LOS mode, the transmitter and receiver must have a direct line-of-sight, which limits the range of the system. In the diffuse mode, the modulated light is scattered through the environment, by which communication is enabled in the scenario of the non-line-of-sight between the transmitter and receiver. The diffuse mode enables VLC systems to operate in a wide range of indoor environments, where light sources are abundant.

VLC can provide significant benefits over traditional RF wireless technologies, including improved security, lower interference, higher data rates, low-cost devices, low power consumption, and the ability to use existing lighting infrastructure for data transmission. These advantages make VLC an attractive alternative for a variety of applications, such as indoor positioning, augmented reality, internet of things (IoT), health and safety, retail and advertising, and smart homes [1]. However, despite the potential benefits, VLC is still in its early stages of development, and there are several challenges that need to be addressed, such as the design of efficient modulation schemes, the development of reliable receiver systems, and the mitigation of ambient light interference [3].

1.2 Related works and motivation

Ultra-reliable low latency communication (URLLC) is a key feature of 5G and beyond wireless networks that aims to enable ultra-reliable and low-latency communication for mission-critical applications, such as industrial automation, autonomous vehicles, and remote surgery [4], [5]. The goal of URLLC is to provide a communication infrastructure that can support the emerging use cases that demand high reliability and low latency, such as Industry 4.0, smart cities, and e-health [6]. URLLC represents a major shift in the design and operation of wireless networks, which traditionally prioritize high data rates and throughput. Therefore, the short packet communication (SPC) was invented to for 5G and beyond wireless networks.

Short packet communication is a critical component of URLLC, as many mission-critical applications involve the exchange of small data packets with low latency and high reliability. SPC requires new approaches to channel coding, modulation, multiple access, and error correction, which must be optimized for low latency, high reliability, and low energy consumption [7]. Therefore, Shannon capacity cannot be appropriate for determining the achievable rate in the finite block-length transmission [7]. Due to very short length of packet in SPC, block error rate (BLER) cannot be neglected in the achievable rate in finite the finite block-length transmission [7], [8]. Thus, in the SPC, the function of the achievable rate is presented in terms of the signal-to-noise ratio (SNR), block-length, and block error rate (BLER) [7], [8]. The SPC has been extensively investigated in RF systems for various scenarios, including quasi-static MIMO fading channels [8], broadcast channel [9], channel coding schemes [10], medium access control (MAC) channel [11], latency-critical packet scheduling [12], and mission-critical IoT applications [13]. SPC was employed

in [14] to improve efficiency of data transmission and increase the throughput of spectrum sharing networks. The study in [15] optimizes the long-term power to achieve the maximum achievable rate in the presence of additive white Gaussian noise (AWGN) and quasi-static channel, assuming perfect channel state information (CSI). In [16], an energy-efficient packet scheduling is proposed for SPC, and delay is constrained for optimizing the packet transmission power and code block-length. However, in VLC systems, SPC has been rarely studied.

Conventional orthogonal multiple access (OMA) techniques consist of time division multiple access (TDMA), code division multiple access (CDMA), frequency division multiple access (FDMA), and orthogonal frequency division multiple access (OFDMA). In conventional multiple access, users are served in orthogonal resources (i.e., time slots, frequencies, and bandwidth) to avoid user interference. However, orthogonal frequency division multiplexing (OFDM) and OFDMA are not directly implemented in VLC systems, since real and non-negative signals are required for intensity modulation and direct detection (IM/DD). The utilization of Hermitian symmetry was introduced for real signals, and then direct current (DC) bias and clipping techniques were implemented for non-negative signals to OFDM and OFDMA in VLC systems [17]. Due to reuse of resources in OMA, the performance of multiuser systems is not efficient. Therefore, non-orthogonal multiple access (NOMA) was proposed for more efficient resource utilization. By using power-domain NOMA, message signals for multiple users are multiplexed and transmitted at the same time and frequency.

NOMA is considered as the potential multiple access technique for 5G and beyond. NOMA utilizes superposition coding to multiplex message signals in the power domain at the transmitter, and the receiver uses successive interference cancellation

(SIC) to decode the message signals. According to power domain NOMA, the allocation of power for message signals of users is based on the channel quality. The power coefficients for message signals of low channel users is higher than those of strong channel users. Thus, NOMA can simultaneously support multiple users at the same time-frequency resource. In RF systems, research on NOMA has been conducted in various contexts, such as wireless energy transfer [18], MIMO system [19], multiple-antenna relaying networks [20], and cognitive radio [21]. Recently, implementation and application of NOMA in VLC systems have been studied to improve system performance in terms of latency and spectrum efficiency [22]. In [23], the NOMA in VLC system is first proposed to improve achievable throughput, where channel conditions of users are investigated for efficient and fair power allocation. Author of [24] showed that NOMA provided higher data rate than OMA in VLC system with perfect channel state information (CSI) scenario. In [25], the performance of NOMA in VLC system was evaluated in noisy and outdated CSI in term of the bit-error-rate (BER). NOMA was employed in MIMO VLC system to support multiple users and increase sum rate in [26]. Authors of [27] proposed a light fidelity (LiFi) – enabled bidirectional internet of things (IoT) using NOMA to increase energy efficiency, and results showed that NOMA outperformed OMA with typical channel-based power allocation strategies. Since IM/DD is adapted in the VLC systems, the research on NOMA in VLC systems is still attractive in academia.

The integration of SPC and NOMA has been conducted in RF for URLLC and massive connectivity [27], [28]. Since the requirement of signal for IM/DD in VLC systems is the main difference from RF system, the implementation of SPC in NOMA VLC systems should be carefully investigated. In the prior works, data rate was only evaluated in the NOMA VLC systems [23], [24]. In contrast, the reliability

and latency, which are the stringent requirements of URLLC applications, were not interested. In addition, supporting a large number of users at one time-frequency slot increases the complexity of SIC operation which increases the delay in signal processing at users. As a result, a hybrid NOMA/OMA scheme was proposed in [29] to serve multiple paired users by which each paired user is supported in one orthogonal resource blocks. However, the SPC in NOMA VLC systems is rarely studied. Motivated by this, this thesis evaluates the performance of SPC in NOMA VLC systems for 5G and URLLC applications.

1.3 Contribution

In this thesis, a framework of SPC in NOMA VLC system is proposed to improve reliability and latency. Based on this, the performance of the proposed system is evaluated in terms of reliability, latency, and throughput. The contributions of this thesis are listed as below:

- The SPC is implemented in NOMA VLC systems for URLLC applications. The analytical results of the proposed system indicate that the reliability increases quickly at the medium and high SNR.
- The Gaussian-Chebyshev quadrature method is used to approximate the analytical expression of the average BLER. Subsequently, approximate expressions for reliability, latency, and throughput are derived.
- The evaluation of reliability and latency in NOMA VLC systems considers SPC and long-packet communication (LPC). A comparison between the SPC-

NOMA VLC system and the LPC-NOMA VLC system is presented for benefits of SPC for URLLC applications.

- An analysis is conducted to evaluate the reliability, latency, and throughput of both SPC-NOMA VLC and SPC-OMA VLC systems' performance.
- The impact of selecting LEDs with different semi-angles on the sum throughput is assessed in the context of the SPC-NOMA VLC system.
- The numerical search method is utilized to determine the optimal values of transmission rates and power allocation coefficients that maximize the sum throughput of the SPC-NOMA VLC system.

1.4 Thesis Organization

This thesis is organized as follows. In Chapter 2, the preliminaries of SPC in RF and VLC systems are discussed. Then, the implementations of SPC in both NOMA and OMA in VLC systems is introduced with performance evaluation and simulation results. Moreover, the comparisons of SPC in NOMA versus OMA in VLC systems and SPC versus long packet communication (LPC) are provided. Chapter 3 presents the optimization problem and the design for maximum system throughput of SPC-NOMA VLC systems, and optimal results are shown with both analysis and simulation. Finally, chapter 4 is conclusion of this thesis.

Chapter 2

SPC-NOMA VLC system

2.1 Preliminary

2.1.1 System model

This study encompasses the transmission of a downlink broadcast channel in an indoor environment. To present an effective evaluation of system performance, we utilize a VLC system comprised of one LED and two users. A schematic of the system model is provided in Figure 2.1, in which the LED is positioned on the ceiling to serve two single-photodiode users. The channel is either static or quasi-static, such that the channel state remains unchanged during transmission. We assume that both the LED and users have perfect knowledge of the channel state information (CSI). The users are uniformly distributed in a circular area. The received signals at the receiver side comprise of both line-of-sight (LOS) components and diffuse

2.1.2 Short packet communication (SPC)

SPC in RF systems

In the RF system, the message signal x_s of the SPC is directly transmitted from the source to the destination. The signal at the receiver is presented as

$$y = Px_s|h|^2 + \mu_D, \quad (2.1)$$

where $|h|$ is magnitude of the channel gain, P is the electrical power of the message signal, and μ_D is the additive white Gaussian noise (AWGN) with the variance σ^2 . In the SPC, each packet is transmitted in message signals. Each packet contains the information bits and addition bits (or metadata) for correct functioning [5]. The BLER of the detection at the receiver is approximated by [7, Eq. (59)]

$$\varepsilon \approx Q \left(\frac{C(\gamma) - R}{\sqrt{V(\gamma)/N}} \right), \quad (2.2)$$

where $\gamma = P|h|^2/\sigma^2$ is the received signal-to-noise ratio (SNR), N is the block-length ($N \geq 100$), $R = k/N$ is the transmission rate, k is the number of information bits in a packet, $C(\gamma) = \log_2(1 + \gamma)$ is the Shannon capacity, and $V(\gamma) = (1 - (1 + \gamma)^{-2}) (\log_2 e)^2$ is the channel dispersion, and $Q(\cdot)$ is Gaussian Q-function, with $Q(x) = \int_x^\infty e^{-t^2/2} dt$.

The average BLER is calculated by

$$\bar{\varepsilon} \approx E \left\{ Q \left(\frac{C(\gamma) - R}{\sqrt{V(\gamma)/N}} \right) \right\} = \int_{-\infty}^{\infty} Q \left(\frac{C(\gamma) - R}{\sqrt{V(\gamma)/N}} \right) f_\gamma(x) dx, \quad (2.3)$$

where $E\{\cdot\}$ is expectation, and $E\{X\} = \int_{-\infty}^{\infty} x f_X(x) dx$.

SPC in VLC systems

For VLC systems that use intensity modulation and direct detection (IM/DD), the transmitted signals must be real and non-negative. When implementing SPC in VLC systems, Hermitian symmetry is employed to achieve real signals. Additionally, a DC bias is added to the LED to ensure non-negative signals for transmission. The message signal at the LED is then represented by

$$x_{\text{LED}} = \sqrt{P}x_s + V_{\text{DC}}. \quad (2.4)$$

After removing DC bias at the receiver, the received signal is given as

$$y = \sqrt{P}hx_s + \mu_0, \quad (2.5)$$

where μ_0 is zero mean real-valued AWGN with σ_0^2 . After removing DC bias at the receiver, the SNR at U_i is given by

$$\gamma_i = \gamma_{\text{Tx}}h_i^2. \quad (2.6)$$

Due to the utilization of Hermitian symmetry, the scaling factor 0.5 is multiplied with the Shannon capacity $C(\gamma_i)$ and channel dispersion $V(\gamma_i)$ in the expression of the BLER of the SPC in the VLC system. The BLER of the SPC in the VLC system

at U_i ($i \in \{1, 2\}$) is approximated by [22], [31]

$$\varepsilon_i \approx Q \left(\frac{0.5C(\gamma_i) - R_i}{\sqrt{0.5V(\gamma_i)/N_i}} \right), \quad (2.7)$$

where N_i , k_i , and R_i are block-length, number of information bits allocated to U_i , and transmission rate at U_i , respectively.

2.1.3 NOMA in VLC systems

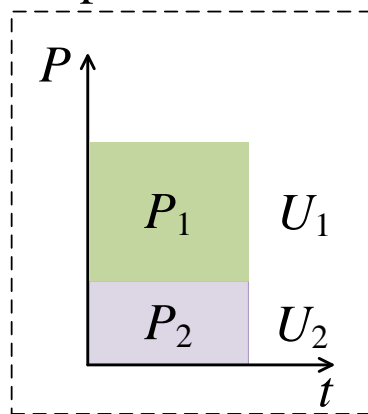
The principle of NOMA schemes is based on the channel quality, shown in Figure 2.2. We consider that two users are scheduled in one cluster and served in a resource block¹. We define that the far user U_1 has lower channel gain, and the near user U_2 has higher channel gain. The message signals for users is superposed in the power domain. The poorer the user's channel is, the higher power coefficient is allocated. After Hermitian symmetry and adding DC bias [24], [30], the superposed signal at one LED is given by

$$x_{\text{LED}} = \sqrt{a_1 P} s_1 + \sqrt{a_2 P} s_2 + V_{\text{DC}}, \quad (2.8)$$

where V_{DC} is the DC bias added for non-negative unipolar signal, s_1 and s_2 are the intended message signal for U_1 and U_2 , and a_1 and a_2 are the power coefficients allocated to the message signals of U_1 and U_2 . Total power allocation coefficients must satisfy: $a_1 + a_2 = 1$ and $a_1 \geq a_2$.

¹When there are more than two users in the system, users are sorted and paired, and the hybrid NOMA/OMA is used to support multiple user pairs. The power domain NOMA multiplexes two users of each pair. User pairs are multiplexed by the OMA scheme. When the number of users is odd, users are sorted and paired, and the remaining unpairing one is supported by the separate power and resource block [29].

Superposition in the power domain



VLC System

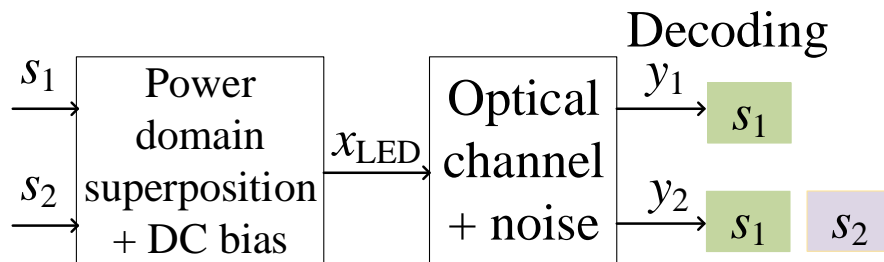
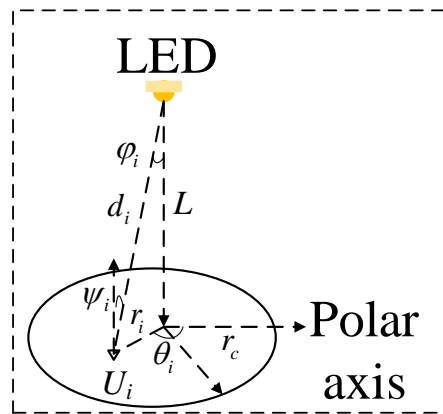


Figure 2.2: Principle of the two-user NOMA and VLC systems.

At U_i ($i \in \{1, 2\}$), DC bias is eliminated, and the received signal is given by

$$y_i = h_i \left(\sqrt{a_1 P} s_1 + \sqrt{a_2 P} s_2 \right) + \mu_i, \quad (2.9)$$

where μ_i is the zero-mean real-valued AWGN with the variance σ_i^2 and h_i is the channel gain between the LED and U_i . After optical-to-electrical conversion, the signal processing is presented as following.

At U_1 , the SIC is not performed, and the intended signal is directly decoded. The SINR is given by

$$\gamma_{11} = \frac{a_1 h_1^2}{a_2 h_1^2 + 1/\gamma_{\text{Tx}}}, \quad (2.10)$$

where $\gamma_{\text{Tx}} = \frac{P}{\sigma_i^2}$ is the transmitted SNR.

At U_2 , the SIC is performed to remove the interference of the message for U_1 , and the message for U_1 is treated as the interference. The SINR of the intended message for U_2 at U_1 is given by

$$\gamma_{21} = \frac{a_1 h_2^2}{a_2 h_2^2 + 1/\gamma_{\text{Tx}}}. \quad (2.11)$$

The SINR of the own signal for U_2 is given by

$$\gamma_{22} = \frac{a_2 h_2^2}{a_1 h_2^2 \delta_{21} + 1/\gamma_{\text{Tx}}}, \quad (2.12)$$

where $\delta_{21} \in [0, 1]$ is the imperfect SIC factor². In this paper, for the goal of evaluating optimal system performance, we consider $\delta_{21} = 0$.

²In practice, due to the imperfect SIC circuit design and error propagation, the operation of SIC may result in the residual interference, which leads to the degradation of system performance.

2.1.4 OMA in VLC systems

In this paper, we consider that TDMA is adopted to serve users in the orthogonal time resource. The transmitted signal for U_i at one LED is given by

$$x_i = \sqrt{a_i P} s_i + V_{\text{DC}}. \quad (2.13)$$

Equation (2.13) assumes that there is no interference at U_i caused by other users in the OMA VLC system. After removing DC bias, the received signal at U_i is presented by

$$y_i = \sqrt{a_i P} h_i s_i + \mu_i. \quad (2.14)$$

Then, the received SNR at U_i is given by

$$\gamma_i^o = \frac{a_i P h_i^2}{\sigma_i^2} = a_i h_i^2 \gamma_{Tx}. \quad (2.15)$$

2.1.5 VLC channel and distribution of received signal-to-noise ratio

The power allocation strategy for all users at the transmitter is based on the knowledge of the channel quality. In the two-user NOMA system, the channel gain quality is assumed to be ordered as

$$h_1 \leq h_2. \quad (2.16)$$

The positions of receivers are assumed to be uniformly distributed within the circular area under the LED. The cell radius is denoted by r_c . The vertical distance between

the LED and users on the circle plane is denoted by L . In the polar coordinate system, the position of U_i is presented by (r_i, θ_i) , where r_i is horizontal distance from the LED to the receiver and θ_i is the polar angle from the polar axis. The channel gain between U_i and the LED is given by

$$h_i = \frac{(m+1)AR_p}{2\pi d_i^2} \cos^m(\phi_i) T(\psi_i) g(\psi_i) \cos(\psi_i), \quad (2.17)$$

where Lambertian radiation pattern is given by $m = -\ln(2)/\ln(\cos(\Phi_{1/2}))$; $\Phi_{1/2}$ is the semi-angle of the LED; Ψ_{FOV} is the field-of-view (FOV) semi-angle of the photodiode (PD) at each receiver; A is detection area of the PD; R_p is the responsivity of the PD; d_i is the Euclidean distance between the receiver and the LED; ψ_i is the angle of irradiance; ϕ_i is the angle of incidence; $T(\psi_i)$ is the gain of optical filter at the receiver; and $g(\psi_i)$ is the gain of the optical concentrator at the receiver, given by

$$g(\psi_i) = \begin{cases} \frac{n^2}{\sin^2(\Psi_{\text{FOV}})}, & 0 \leq \psi_i \leq \Phi_{\text{FOV}}, \\ 0, & \psi_i > \Phi_{\text{FOV}}, \end{cases} \quad (2.18)$$

where n is the refractive index of the optical concentrator, $n \in [1, 2]$.

From Figure 2.1, the Euclidian distance between the LED and U_i , the angle of irradiance, and the angle of incidence are calculated by $d_i = \sqrt{r_i^2 + L^2}$, $\cos(\phi_i) = L/\sqrt{r_i^2 + L^2}$, and $\cos \psi_i = L/\sqrt{d_i^2 + L^2}$, respectively. With the uniform distribution, the probability density function (PDF) of a location in a circle is given by $f_{r_i}(r) = 2r/r_c^2$.

According to [24], the unordered PDF of received SNR at U_i is obtained by using

the method of transformation and the change of variable method [32, Chap. 6] as

$$f_{\gamma_i}(x) = \frac{1}{r_c^2} \frac{1}{m+3} (\mathcal{C}(m+1)L^{m+1})^{\frac{2}{m+3}} \left(\frac{1}{\gamma_{\text{Tx}}}\right)^{-\frac{1}{m+3}} x^{-\frac{m+4}{m+3}}, \quad (2.19)$$

where $\mathcal{C} = \frac{1}{2\pi} AT(\psi_i)g(\psi_i)$ and $\gamma_i = \gamma_{\text{Tx}}h_i^2$. Since $h_i^2 \in [h_{\min}^2, h_{\max}^2]$, $h_{\min}^2 = (\mathcal{C}(m+1)L^{m+1})^2 / (r_c^2 + L^2)^{(m+3)}$, and $h_{\max}^2 = (\mathcal{C}(m+1)L^{m+1})^2 / L^{2(m+3)}$, then $\gamma_i \in [\gamma_{\min}, \gamma_{\max}] = [\gamma_{\text{Tx}}h_{\min}^2, \gamma_{\text{Tx}}h_{\max}^2]$. The cumulative distribution function (CDF) of the received SNR at U_i is obtained by integrating (2.19) with respect to $x \in [\gamma_{\min}, \gamma_{\max}]$. The unordered CDF of the received SNR is given as

$$F_{\gamma_i}^\gamma(x) = \frac{1}{r_c^2} \frac{1}{m+3} (\mathcal{C}(m+1)L^{m+1})^{\frac{2}{m+3}} \left(\frac{1}{\gamma_{\text{Tx}}}\right)^{-\frac{1}{m+3}} x^{-\frac{1}{m+3}} + \frac{L^2}{r_c^2} + 1. \quad (2.20)$$

Since the channel quality is ordered for the power allocation, the ordered statistics [24], [32, Chap. 6], [33] are considered in this paper. The ordered CDF of the received SINR at U_i is presented by

$$\begin{aligned} F_{\gamma_i}(x) &= \sum_{\hat{j}=i}^2 \frac{2!}{(2-\hat{j})!\hat{j}!} (F_{\gamma_i}^\gamma(x))^{\hat{j}} (1 - F_{\gamma_i}^\gamma(x))^{2-\hat{j}} \\ &= \sum_{\hat{j}=i}^2 \frac{2!}{(2-\hat{j})!\hat{j}!} \left(-\omega x^{-\frac{1}{m+3}} + \frac{L^2}{r_c^2} + 1\right)^{\hat{j}} \left(\omega x^{-\frac{1}{m+3}} - \frac{L^2}{r_c^2}\right)^{2-\hat{j}}, \end{aligned} \quad (2.21)$$

where $\omega = \frac{1}{r_c^2} (\mathcal{C}(m+1)L^{m+1})^{\frac{2}{m+3}} \left(\frac{1}{\gamma_{\text{Tx}}}\right)^{-\frac{1}{m+3}}$.

2.2 Performance analysis

2.2.1 Average BLER in VLC systems

The average BLER of the SPC in the VLC system is approximated by

$$\bar{\varepsilon}_i \approx E \left\{ Q \left(\frac{0.5C(\gamma_i) - R_i}{\sqrt{0.5V(\gamma_i)/N_i}} \right) \right\} = \int_0^\infty Q \left(\frac{0.5C(\gamma_i) - R_i}{\sqrt{0.5V(\gamma_i)/N_i}} \right) f_{\gamma_i}(x) dx. \quad (2.22)$$

Since the received SNR is limited in the circle area under the LED, then $\gamma \in [\gamma_{\min}, \gamma_{\max}]$. The average BLER is approximated by

$$\bar{\varepsilon}_i \approx \int_{\gamma_{i,\min}}^{\gamma_{i,\max}} Q \left(\frac{0.5C(\gamma_i) - R_i}{\sqrt{0.5V(\gamma_i)/N_i}} \right) f_{\gamma_i}(x) dx. \quad (2.23)$$

Using partial integral, (2.23) is expressed by

$$\bar{\varepsilon}_i = F_{\gamma_i}(x) Q \left(\frac{\log_2(1+x) - 2R_i}{\sqrt{2 \left(1 - \frac{1}{(1+x)^2}\right) (\log_2 e)^2 / N_i}} \right) \Bigg|_{\gamma_{i,\min}}^{\gamma_{i,\max}} - \int_{\gamma_{i,\min}}^{\gamma_{i,\max}} F_{\gamma_i}(x) \zeta(x) dx, \quad (2.24)$$

where $F_{\gamma_i}(x)$ is cumulative distribution function (CDF) of the variable x , and $\zeta(x)$ is the first order derivative of the BLER expression, and $\frac{dQ(f(x))}{dx} = -\frac{1}{\sqrt{2\pi}} \frac{df(x)}{dx} e^{-f(x)^2/2}$.

The function $\zeta(x)$ is expressed by

$$\zeta(x) = -\frac{1}{\sqrt{2\pi}} \left(\frac{\sqrt{N_i/2}}{(1+x)\sqrt{\left(1-\frac{1}{(1+x)^2}\right)}} - \frac{\sqrt{N_i/2}(\log_2(1+x) - 2R_i)}{\log_2 e \left(1-\frac{1}{(1+x)^2}\right)^{3/2} (1+x)^3} \right) \quad (2.25)$$

$$\times e^{-\frac{1}{2} \left(\frac{\log_2(1+x) - 2R_i}{\sqrt{2\left(1-\frac{1}{(1+x)^2}\right)} (\log_2 e)^2 / N_i} \right)^2}.$$

It is complicated to derive the close-form expression of the remaining integral in (2.24). The average BLER is approximated by using the Gaussian-Chebyshev quadrature method as [34, Table 25.4]

$$\begin{aligned} \bar{\varepsilon}_i \triangleq f(\gamma_{i,\max}, \gamma_{i,\min}, N_i, R_i) &= Q \left(\frac{0.5C(\gamma_{i,\max}) - R_i}{\sqrt{0.5V(\gamma_{i,\max})/N_i}} \right) F_{\gamma_i}(\gamma_{i,\max}) \\ &- Q \left(\frac{0.5C(\gamma_{i,\min}) - R_i}{\sqrt{0.5V(\gamma_{i,\min})/N_i}} \right) F_{\gamma_i}(\gamma_{i,\min}) \\ &- \nu_i \sum_{v=1}^{\bar{V}} \frac{\pi}{\bar{V}} \sqrt{1 - \cos^2 \left(\frac{(2v-1)\pi}{2\bar{V}} \right)} F_{\gamma_i} \left(\nu_i \cos \left(\frac{(2v-1)\pi}{2\bar{V}} \right) + \vartheta_i \right) \\ &\times g \left(\nu_i \cos \left(\frac{(2v-1)\pi}{2\bar{V}} \right) + \vartheta_i \right), \end{aligned} \quad (2.26)$$

where \bar{V} is the complexity-accuracy trade-off parameter, $\nu_i = \frac{\gamma_{i,\max} - \gamma_{i,\min}}{2}$, and $\vartheta_i = \frac{\gamma_{i,\max} + \gamma_{i,\min}}{2}$.

Reliability at U_i is the probability that the packet is correctly detected, given by

$$\chi = (1 - \varepsilon_i)100\%. \quad (2.27)$$

Throughput at U_i is the number of correctly determined information bits at the

receiver per transmission, presented by

$$T_i = \frac{N_i}{N} R_i (1 - \varepsilon_i). \quad (2.28)$$

Latency at U_i is the delay in transmissions, given by

$$\ell = \frac{NT_c}{1 - \varepsilon_i}, \quad (2.29)$$

where T_c is the duration of a block.

2.2.2 SPC in NOMA VLC systems

In NOMA transmission strategy, the allocated block-length for U_1 and U_2 is $N_1 = N_2 = N$, since the LED transmits signal to two users simultaneously with the different power allocation. At the receiver side, the SIC is performed at U_2 to remove the interference of the U_1 message in the received signal, and then U_2 decodes its message. At U_1 , the message of U_2 is treated as the interference, and U_1 directly decodes its own message in the received signal.

Signal processing at U_1

The signal-to-noise-plus-interference ratio (SINR) of the message signal at U_1 is given by

$$\gamma_{11} = \frac{a_1 P h_1^2}{a_2 P h_1^2 + \sigma^2} = \frac{a_1}{a_2 + 1/\gamma_1}. \quad (2.30)$$

Since $\gamma_1 \in [\gamma_{\min}, \gamma_{\max}]$, then $\gamma_{11} \in [\gamma_{11,\min}, \gamma_{11,\max}] = \left[\frac{a_1}{a_2 + 1/\gamma_{\min}}, \frac{a_1}{a_2 + 1/\gamma_{\max}} \right]$. From (2.21) and (2.30), the ordered CDF of the received SINR of the message signal U_1 is

given by

$$F_{\gamma_{11}}(x) = 2 \left(-\omega \left(\frac{x}{a_1 - a_2 x} \right)^{-\frac{1}{m+3}} + \frac{L^2}{r_c^2} + 1 \right) - \left(-\omega \left(\frac{x}{a_1 - a_2 x} \right)^{-\frac{1}{m+3}} + \frac{L^2}{r_c^2} + 1 \right)^2. \quad (2.31)$$

Power coefficients a_1 and a_2 must satisfy the condition: $a_1 - a_2 x > 0$. From (2.26), (2.30) and (2.31), the average BLER of U_1 is approximated by

$$\bar{\varepsilon}_{11} = f(\gamma_{11,\max}, \gamma_{11,\min}, N_1, R_1). \quad (2.32)$$

Signal processing at U_2

The SIC performs to detect message signal for U_1 first, and then detect message signal for U_2 . The SINR of the message signal of U_1 in U_2 is given by

$$\gamma_{21} = \frac{a_1 P h_2^2}{a_2 P h_2^2 + \sigma^2} = \frac{a_1}{a_2 + 1/\gamma_2}. \quad (2.33)$$

Since $\gamma_2 \in [\gamma_{\min}, \gamma_{\max}]$, then $\gamma_{21} \in [\gamma_{21,\min}, \gamma_{21,\max}] = \left[\frac{a_1}{a_2 + 1/\gamma_{\min}}, \frac{a_1}{a_2 + 1/\gamma_{\max}} \right]$. From (2.21) and (2.33), the ordered CDF of the received SINR of the message signal of U_1 at U_2 is given by

$$F_{\gamma_{21}}(x) = \left(-\omega \left(\frac{x}{a_1 - a_2 x} \right)^{-\frac{1}{m+3}} + \frac{L^2}{r_c^2} + 1 \right)^2. \quad (2.34)$$

Using (2.26), (2.33) and (2.34), the average BLER of U_1 at U_2 is approximated by

$$\bar{\varepsilon}_{21} = f(\gamma_{21,\max}, \gamma_{21,\min}, N_1, R_1). \quad (2.35)$$

The SINR of the message signal of U_2 at U_2 is given as

$$\gamma_{22} = \frac{a_2 P h_2^2}{\sigma^2} = a_2 \gamma_2. \quad (2.36)$$

Since $\gamma_2 \in [\gamma_{\min}, \gamma_{\max}]$, then $\gamma_{22} \in [\gamma_{22,\min}, \gamma_{22,\max}] = [a_2 \gamma_{\min}, a_2 \gamma_{\max}]$. From (2.21) and (2.36), the ordered CDF of SINR U_2 at U_2 is given by

$$F_{\gamma_{22}}(x) = \left(-\omega \left(\frac{x}{a_2} \right)^{-\frac{1}{m+3}} + \frac{L^2}{r_c^2} + 1 \right)^2. \quad (2.37)$$

Based on (2.26), the average BLER of the message U_2 at U_2 is approximated by

$$\bar{\varepsilon}_{22} = f(\gamma_{22,\max}, \gamma_{22,\min}, N_2, R_2). \quad (2.38)$$

The overall average BLER of U_2 is approximated by

$$\bar{\varepsilon}_2 = \bar{\varepsilon}_{21} + (1 - \bar{\varepsilon}_{21}) \bar{\varepsilon}_{22}. \quad (2.39)$$

2.2.3 SPC in OMA VLC systems

In OMA systems, since two users are assigned to the different orthogonal resources, there is no interference at U_1 (or U_2) caused by U_2 (or U_1). The power allocation to each user is based on the channel quality. N_1 and N_2 are the allocated block-length for U_1 and U_2 , and $N_1 + N_2 = N$. At U_i ($i \in \{1, 2\}$), the SNR is given by

$$\gamma_i^o = \frac{a_i P h_i^2}{\sigma^2} = a_i \gamma_i. \quad (2.40)$$

Table 2.1: SIMULATION PARAMETERS

Symbol	Name of parameters	Value
L	Vertical distance from LED to circular area	2.5 m
r_c	Cell radius	3.5 m
K	Total number of users	2
$\Phi_{1/2}$	LED semi-angle	60°
Ψ_{FOV}	PD FOV	60°
R_p	PD responsibility	0.4 A/W
A	PD detection area	1 cm ²
n	Reflective index	1.5
T	Optical filter gain	1
T_c	Duration time of a block	1 μ s

Since $\gamma_i \in [\gamma_{\min}, \gamma_{\max}]$, then $\gamma_i^o \in [\gamma_{i,\min}, \gamma_{i,\max}] = [a_i\gamma_{\min}, a_i\gamma_{\max}]$. Following (2.21) and (2.40), the ordered CDF of the received SNR at U_i is also presented as

$$F_{\gamma_i^o}(x) = \sum_{\hat{j}=i}^2 \frac{2!}{(2-\hat{j})!\hat{j}!} \left(-\omega \left(\frac{x}{a_i} \right)^{-\frac{1}{m+3}} + \frac{L^2}{r_c^2} + 1 \right)^{\hat{j}} \left(\omega \left(\frac{x}{a_i} \right)^{-\frac{1}{m+3}} - \frac{L^2}{r_c^2} \right)^{2-\hat{j}}. \quad (2.41)$$

The average BLER at U_i is approximated by

$$\bar{\varepsilon}_i^o = f(\gamma_{i,\max}^o, \gamma_{i,\min}^o, N_i, R_i). \quad (2.42)$$

2.3 Numerical results

In this section, we present numerical results and utilize Monte Carlo simulations to verify the analysis in Section 2.2. The benefits of the SPC in terms of reliability and latency are shown in the comparison between SPC and LPC in NOMA VLC systems. To demonstrate the effectiveness of the proposed system, we compare the

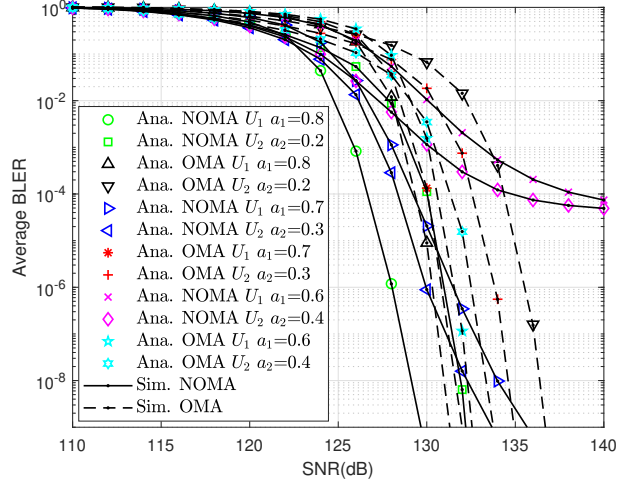


Figure 2.3: Average BLER comparison between NOMA versus OMA using SPC with different power allocation strategies.

performance of the SPC in NOMA and OMA VLC systems, and discuss the effect of the semi-angles of the LEDs to the system throughput of the SPC in the NOMA VLC system. The parameters of the channel gains are shown in Table 2.1. In the simulation, we choose the block-length $N_1 = N_2 = 200$, $k_1 = k_2 = 80$ bits for NOMA scheme, and $N_1 = N_2 = 100$, $k_1 = k_2 = 80$ bits for OMA scheme. In comparison of the SPC-NOMA VLC to SPC-OMA VLC, the power allocation strategies are $a_1 = 0.8$ and $a_2 = 0.2$, and the value of SNR for the transmission is $\gamma_{Tx} = 130$ dB.

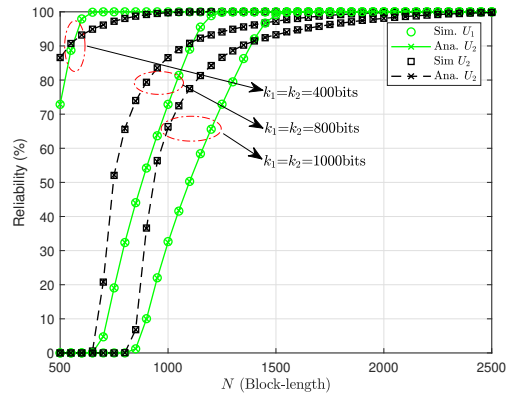
Figures 2.3-2.8 show performances of the proposed system. In these figures, ‘Ana.’ and ‘Sim.’ denote analytical and simulation results, respectively. The analytical results are matched with the simulation results.

Figure 2.3 illustrates the impact of power allocation on the block error rate (BLER) performance of users in both NOMA and OMA systems. The simulation results match well with the analytical results obtained at different power allocation

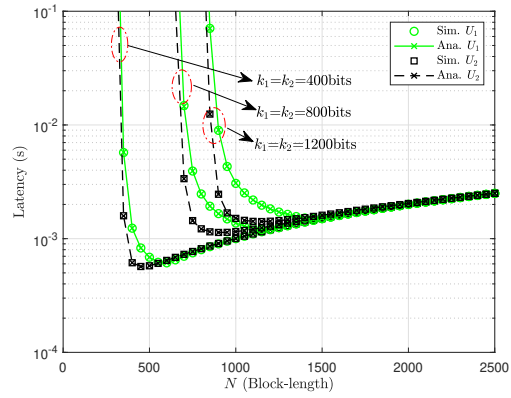
coefficients. In the SPC-OMA system, the BLER of U_1 is consistently lower than that of U_2 since there is no interference from other users. At low SNR levels (110-120 dB), the BLER decreases slowly in both systems. At medium SNR levels (120-130 dB), the BLER of the SPC-NOMA system decreases more rapidly than that of the SPC-OMA system, with the former achieving a BLER of less than 10^{-5} at 130 dB. When $a_1 = 0.6$ and $a_2 = 0.4$, the SPC-OMA system can achieve a BLER of less than 10^{-5} , while the BLER of the SPC-NOMA system cannot be less than 10^{-5} . Increasing the power allocation for the far user in the NOMA system improves the BLER performance since interference at the near user caused by the far user decreases. The SPC-NOMA system can achieve the desired error probability at 131 dB, while the SPC-OMA system requires 135 dB for all users. Therefore, the use of SPC in the NOMA system requires less power than in the OMA system, and the NOMA system's performance is enhanced when power allocation is increased for the far user.

Figure 2.4 compares the reliability and latency of short packets (400 bits) and long packets (800 bits and 1000 bits) in a NOMA VLC system. The reliability and latency are calculated as a function of the total block-length at $\gamma_{\text{Tx}} = 130$ dB. The reliability of short messages is higher than that of longer messages. With over 1500 block-length, SPC can meet the reliability requirement, whereas LPC needs over 2500 block-length to meet the same requirement. The latency of short messages is lower than that of longer messages. SPC can achieve sub-millisecond latency, while the latency of the LPC system is more than one millisecond. The use of SPC can satisfy both reliability and latency requirements.

In Figure 2.5, the reliability for U_1 is higher than that of U_2 at both NOMA and OMA systems in the range of the medium SNR. At high SNR, the reliability of U_2



(a)



(b)

Figure 2.4: SPC and LPC for NOMA VLC.

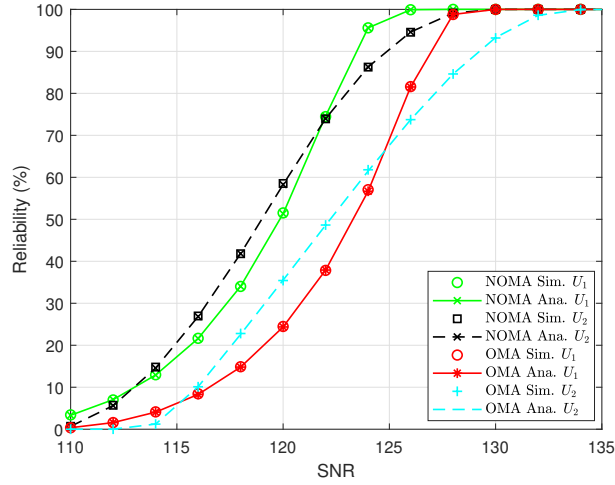


Figure 2.5: The reliability of the SPC in NOMA and OMA VLC system.

is higher than that of U_1 , which indicates that U_2 can only achieve high reliability when transmitted power is high. The required SNR to achieve the desired reliability is lower in NOMA systems (130 dB) than in OMA systems (135 dB). The reliability of the system not only depends on the transmitted SNR but also on the transmission rate, as shown in Equation (2.7). In the SPC-NOMA VLC system, the LED serves two users simultaneously with $N_1 = N_2 = N$, whereas the LED in the SPC-OMA VLC system serves two users in orthogonal time slots with $N_1 = N_2 = N/2$. The transmission rate of each user in the SPC-NOMA VLC system is always lower than that of the SPC-OMA VLC system. As a result, the SPC-NOMA VLC system provides higher reliability.

Figure 2.6 compares the latency of users in the SPC-NOMA and SPC-OMA VLC systems. The latency at U_2 is similar in both NOMA and OMA systems. However, the latency at U_1 in the NOMA system is approximately half of that in the OMA system. Therefore, the SPC-NOMA VLC system reduces latency for the

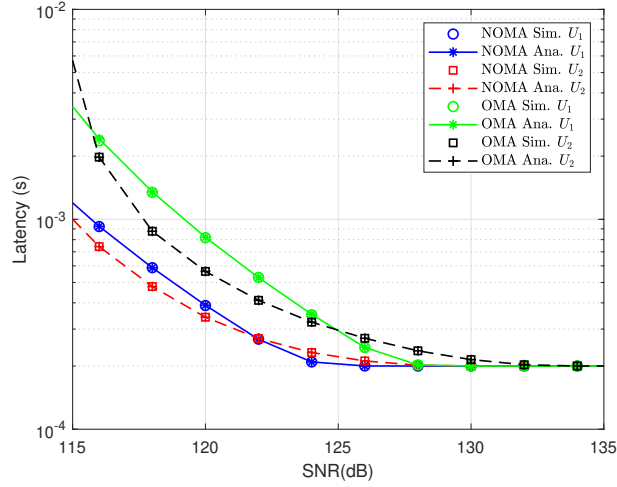


Figure 2.6: Latency comparison between NOMA versus OMA using SPC.

users. Additionally, the NOMA system satisfies the latency requirement at a lower SNR compared to the OMA system, specifically at 116 dB for the NOMA system and 119 dB for the OMA system.

Figure 2.7 illustrates the sum throughput and individual user throughput of the NOMA and OMA VLC systems. The sum throughput of the NOMA system is greater than that of the OMA system. The maximum sum throughput of the NOMA system is attained at 130 dB, whereas the OMA system attains its maximum sum throughput at 134 dB. Since SIC is implemented at U_2 in the NOMA system, the throughput of U_2 is higher than that of U_1 at low SNR. At high SNR, the far user has a higher throughput. The throughput at each user is determined by the transmitted power, transmission rate, block-length for each user, and total block-length. In the NOMA scheme, all users have the same block-length, while the OMA scheme employs the block-length N to serve all users with different allocation of total block-length for each user. The user throughput in the NOMA scheme is higher than that in the

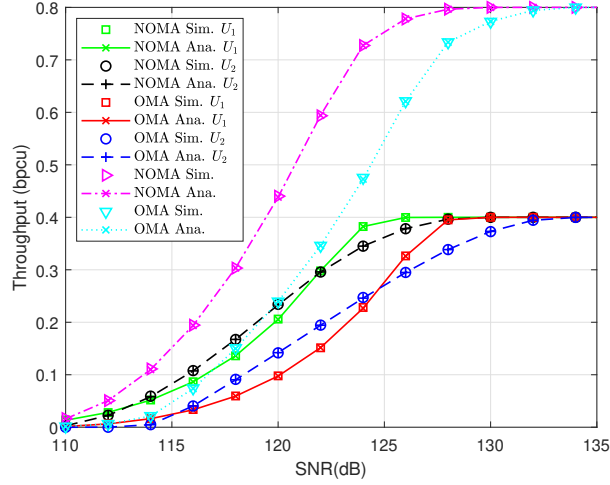


Figure 2.7: Throughput of SPC for NOMA and OMA.

OMA scheme.

Figure 2.8 shows the sum throughput of the SPC in both NOMA and OMA VLC schemes with various semi-angles of the LED. The channel gain depends on the Lambertian radiation pattern, which is determined by the semi-angle of the LED. Thus, the semi-angle of the LED has an impact on the sum throughput of the system. At $\gamma_{Tx} = 120$ dB, the SPC-NOMA VLC system achieves maximum sum throughput at 50° semi-angle, while the SPC-OMA system achieves maximum sum throughput at 40° semi-angle. At $\gamma_{Tx} = 130$ dB, 35° semi-angle LED provides the maximum sum throughput of the SPC-NOMA VLC system, while the optimal semi-angle of the LED for the SPC-OMA VLC system is 45° semi-angle. The optimal semi-angle of the LED depends on the SNR value. A lower semi-angle LED can be useful as the SNR value increases.

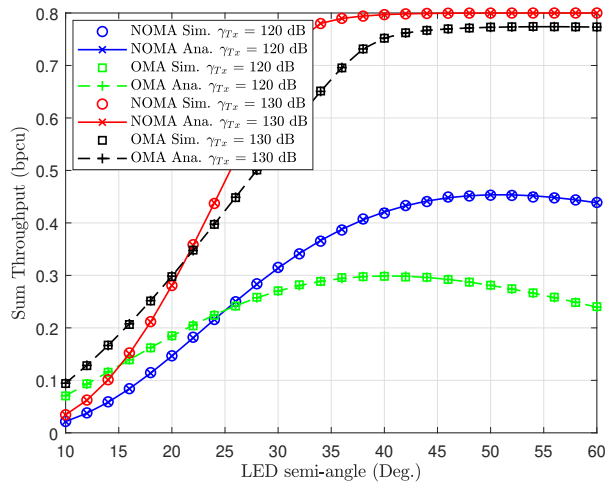


Figure 2.8: The sum throughput for different values of semi-angles at different SNR.

Chapter 3

Optimal sum throughput design

3.1 Optimization problem

In the SPC-NOMA VLC system, the transmitted signals to users are superimposed in the power domain, and the LED serves both U_1 and U_2 simultaneously in the block-length N . It is assumed that $N_1 = N_2 = N$ in NOMA systems. The goal is to obtain maximum sum throughput of the SPC-NOMA VLC system. The optimization problem is formulated as

$$\max_{R_i, a_i} \bar{T} \quad (3.1a)$$

$$\text{s.t.} \quad 0 \leq a_i = 1, i \in \{1, 2\}, \quad (3.1b)$$

$$a_1 + a_2 = 1, \quad (3.1c)$$

$$0 \leq R_i \leq 2.56, \quad (3.1d)$$

where $\bar{T} = T_1 + T_2$. According to (2.7) and (2.28), the sum throughput \bar{T} is formulated as

$$\bar{T} = R_1 (1 - Q(\Xi(\gamma_{11}, R_1))) + R_2 (1 - Q(\Xi(\gamma_{22}, R_2))) (1 - Q(\Xi(\gamma_{21}, R_1))), \quad (3.2)$$

where $\Xi(\gamma_i, R_i) \triangleq \frac{\log_2(1+\gamma_i) - 2R_i}{\log_2 e \sqrt{2 \left(1 - \frac{1}{(1+\gamma_i)^2}\right)^{1/N}}}$. The transmission rates R_i and power allocation coefficients a_i for U_i are determined at the LED, and the transmission rate of U_1 is independent to that of U_2 . We consider the equality $a_1 + a_2 = 1$ in (3.1a), where total power is consumed to transmit signal to all users. According to (3.2), there are three variables in this optimization problem. We need to determine the power allocation and transmission rates to obtain the maximum sum throughput \bar{T} subject to the constraints in (3.2).

3.2 Optimal design

In this section, we present a proposed design for the transmission rates and power allocation strategy, aimed at solving the optimization problem written in equation (3.1). To facilitate this optimization, we examine the two constraints stated in equations (3.1b) and (3.1d). We then provide an analysis of the optimal design for system throughput.

Proposition 3.2.1. *The error probability in (2.7) is monotonically decreasing with SNR/SINR.*

Proof. Please see Appendix A. □

According to (2.7) and (2.28), the effective throughput at each user depends on its power allocation. Following the NOMA principle, there is the trade-off between throughput and power allocation to each user. Since the Q-function is used in the throughput calculation, the optimal power allocation cannot be obtained in closed form. Therefore, the one-dimensional search is used to find the solution close to the optimal solution, where R_1 and R_2 are fixed values.

Proposition 3.2.2. *The error probability in (2.7) is monotonically increasing with the transmission rate R_i .*

Proof. Please see Appendix B. □

Proposition 3.2.3. *The transmission rate at each user is limited in the range $[0, 2.56]$.*

Proof. The transmission rate R is given by $R = k/N$. According to [35], the length of the information bit k of a packet is less than 256 (32 bytes) to get error probability of 10^{-5} . In SPC, the block-length N is longer than 100. Therefore, $R_i \leq 2.56$. (3.1d) is verified. □

Lemma 3.2.4. *The sum throughput \bar{T} does not monotonically increase with R_1 but is concave with respect to R_1 .*

Proof. Please see Appendix C. □

Lemma 3.2.5. *The sum throughput \bar{T} does not monotonically increase with R_1 but is concave with respect to R_2 .*

Proof. Please see Appendix D. □

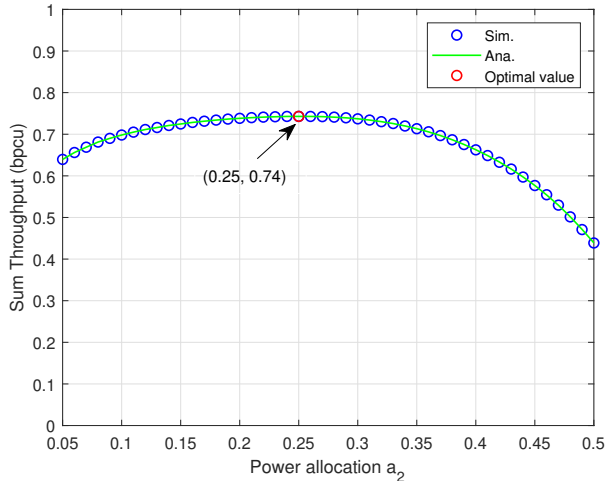


Figure 3.1: Sum throughput as the function of the power allocation for U_2 at $\gamma_{\text{Tx}} = 126$ dB, $R_1 = 0.4$, and $R_2 = 0.35$.

From Appendix C and Appendix D, there exists the optimal transmission rates by solving $\frac{\partial \bar{T}}{\partial R_1} = 0$ and $\frac{\partial \bar{T}}{\partial R_2} = 0$. According (C.2) and (D.2), the optimal solutions cannot be derived in closed form. Due to three variables a_1 , R_1 , and R_2 , we first find the optimal power allocation a_2 by one-dimension search, and then we use two-dimensional search to find the maximum sum throughput with respect to R_1 and R_2 based on the optimal power allocation coefficients derived by one-dimensional search. The optimal results are presented in the next section. We summarize the proposed algorithm to find the optimal solution in **Algorithm 1**.

The accuracy of the proposed method is dependent on the given step size τ . The complexity of the search method is $\mathcal{O}(N_I)$, where N_I is the size of the input values.

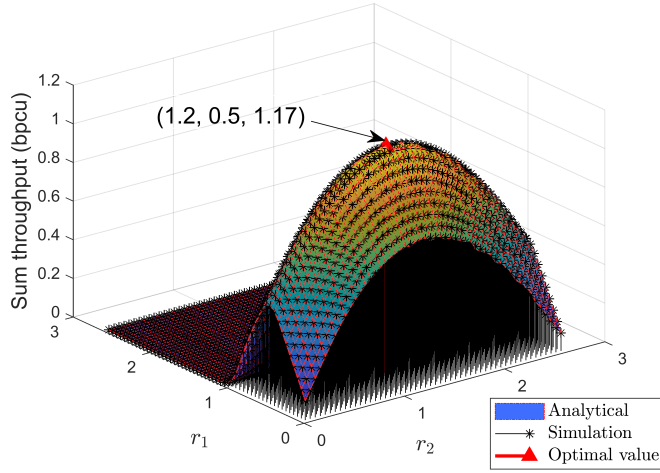


Figure 3.2: Sum throughput for the near user and the maximum throughput point $(R_2, R_1, \bar{T}) = (1.2, 0.5, 1.17)$, $\gamma_{\text{Tx}} = 126$ dB.

3.3 Results

Figure 3.1 illustrates the optimal power allocation obtained through one-dimensional search while the transmission rates of both users are constant. The sum throughput increases from 0 to 0.25 as the power allocation increases, and then it decreases. The decrease in sum throughput is due to a decrease in the throughput of U_2 as its power allocation decreases. Once the optimal power allocation coefficients are obtained, the maximum sum throughputs of both users are derived using a two-dimensional search with varying transmission rates of the two users. The results of the two-dimensional search are shown in Figure 3.2.

Figure 3.2 shows how the sum throughputs are affected by the transmission rates. As shown in equations (2.32), (2.35), (2.38), and (2.39), the throughput of U_1 is independent of the throughput of U_2 , but the throughput of U_2 depends on both R_1 and R_2 . The plot indicates that the sum throughput increases with R_1 in the range

of $R_1 \in [0, 0.5]$ and then decreases with $R_1 > 0.5$. Similarly, the sum throughput increases with R_2 in the range of $[0, 1.2]$ and then decreases with $R_2 > 1.2$. These results verify Lemma 3.2.4 and Lemma 3.2.5 and demonstrate the trade-off between transmission rates and sum throughput. The maximum point on the plot represents a unique parameter-space position that achieves the highest sum throughput. However, according to (2.7), (2.28), and Proposition 3.2.2, the error probability increases with higher transmission rates. Therefore, while a small transmission rate ($R_1 < 0.5$ and $R_2 < 1.2$) results in a low error probability, it also leads to lower sum throughput. On the other hand, a higher transmission rate ($R_1 > 0.5$ and $R_2 > 1.2$) results in higher error probability and lower sum throughput. Therefore, this approach shows that there exists a specific parameter-space position to attain the maximum sum throughput.

Algorithm 1 Algorithm to find optimal power allocation and transmission rates

- 1: **Input:** Initialize vector $a_2 = 0.05 : \tau : 0.5$, with step size $\tau = 0.05$, optimal power allocation $a_2^{opt} = 0$, and maximum sum throughput $\bar{T}_{max} = 0$.
 - 2: **Output:** a_2^{opt} , R_1^{opt} , R_2^{opt}
 - 3: Calculate $\bar{T} \leftarrow \bar{T}(a_2)$ by (3.2) with fixed R_1 and R_2 .
 - 4: **for** $i \leftarrow 1$ to $\text{length}(a_2)$ **do**
 - 5: Set: $\bar{T}_{samp} \leftarrow \bar{T}(i)$.
 - 6: **if** $\bar{T}_{samp} > \bar{T}_{max}$ **then**
 - 7: $\bar{T}_{max} \leftarrow \bar{T}_{samp}$
 - 8: $a_2^{opt} \leftarrow a_2(i)$
 - 9: **end if**
 - 10: **end for**
 - 11: Set $\bar{T}_{max} \leftarrow 0$, $R_1^{opt} = 0$, $R_2^{opt} = 0$, $R_1 = 0.05 : \tau : 2.5$, and $R_2 = 0.05 : \tau : 2.5$.
 - 12: Calculate $\bar{T} \leftarrow \bar{T}(R_1, R_2)$ with optimal power allocation a_2^{opt} and $a_1^{opt} = 1 - a_2^{opt}$ by (3.2).
 - 13: **for** $i \leftarrow \text{length}(R_1)$ **do**
 - 14: **for** $j \leftarrow \text{length}(R_2)$ **do**
 - 15: Set: $\bar{T}_{samp} \leftarrow \bar{T}(i, j)$.
 - 16: **if** $\bar{T}_{samp} > \bar{T}_{max}$ **then**
 - 17: $\bar{T}_{max} \leftarrow \bar{T}_{samp}$
 - 18: $R_1^{opt} \leftarrow R_1(i)$
 - 19: $R_2^{opt} \leftarrow R_2(j)$
 - 20: **end if**
 - 21: **end for**
 - 22: **end for**
-

Chapter 4

Conclusions

In this thesis, we introduced the SPC in a downlink NOMA VLC system with perfect SIC. The SPC-NOMA VLC system was shown to offer higher reliability and lower latency when compared to LPC-NOMA VLC systems. Additionally, our results indicate that the SPC-NOMA VLC system outperforms the SPC-OMA VLC system in terms of reliability, latency, and throughput. We also determined the optimal transmission rates and power allocation strategy to maximize the sum throughput of the SPC-NOMA VLC system for two users. The SPC in VLC systems has the potential to support various URLLC applications, including those in factory automation and intelligent transportation systems.

Appendix A

Proof of proposition 3.2.1

The first partial derivative of ε_i with γ_i is given as

$$\frac{\partial \varepsilon_i}{\partial \gamma_i} = \frac{\partial}{\partial \gamma_i} Q(\Xi(\gamma_i, R_i)) = -\frac{1}{\sqrt{2\pi}} e^{-\frac{1}{2}\Xi^2(\gamma_i, R_i)} \frac{\partial \Xi(\gamma_i, R_i)}{\partial \gamma_i}, \quad (\text{A.1})$$

where $\frac{\partial \Xi(\gamma_i, R_i)}{\partial \gamma_i}$ is the partial derivative of $\Xi(\gamma_i, R_i)$ with respect to γ_i , given by

$$\frac{\partial \Xi(\gamma_i, R_i)}{\partial \gamma_i} = \sqrt{N/2} \frac{1 - \ln 2 \frac{\log_2(1+\gamma_i) - 2R_i}{(1+\gamma_i)^2 - 1}}{\sqrt{(1+\gamma_i)^2 - 1}}. \quad (\text{A.2})$$

It is not clear whether the partial derivative of $\Xi(\gamma_i, R_i)$ with respect to γ_i is positive or negative. Based on (A.2), we define a function, $H(x) = \frac{\log_2 x}{x^2 - 1}$. We find the range of value of $H(x)$ with $x \geq 1$ since $\gamma_i + 1 > 1$. We calculate the first derivative of $H(x)$ with respect to x , given by

$$H'(x) = \frac{h(x)}{(x^2 - 1)^2}, \quad (\text{A.3})$$

where $h(x) = \frac{1}{\ln 2} \left(1 - \frac{1}{x}\right) - 2x \log_2 x$. Since $(x^2 - 1)^2 > 0$ with $x > 1$, the sign of $H(x)$ is the same as $h(x)$. The first derivative of $h(x)$ is given by

$$h'(x) = -\frac{1}{\ln 2} \left(1 - \frac{1}{x^2}\right) - 2 \log_2 x. \quad (\text{A.4})$$

Since $h'(x) < 0$ with $x > 1$, $h(x)$ is a decreasing function with respect to $x > 1$, and $h(x) < h(1) = 0$. $h(x)$ is negative with $x > 1$, and then $H'(x) < 0$ with $x > 1$, which means that $H(x)$ is also a decreasing function with respect to $x > 1$. We determine the value range of $H(x)$ by using L'Hospital's rule, as $\lim_{x \rightarrow 1} H(x) = \frac{1}{2 \ln 2}$ and $\lim_{x \rightarrow \infty} H(x) = 0$. Since $R_i \geq 0$ and $\gamma_i > 0$, we have

$$\begin{aligned} 1 - \ln 2 \frac{\log_2(1 + \gamma_i) - 2R_i}{(1 + \gamma_i)^2 - 1} &\geq 1 - \ln 2 \frac{\log_2(1 + \gamma_i)}{(1 + \gamma_i)^2 - 1} = 1 - \ln 2 H(1 + \gamma_i) \\ &> 1 - \ln 2 \frac{1}{2 \ln 2} = \frac{1}{2} > 0. \end{aligned} \quad (\text{A.5})$$

Since $\frac{\partial \Xi(\gamma_i, R_i)}{\partial \gamma_i} > 0$, $\frac{\partial \varepsilon_i}{\partial \gamma_i} < 0$. Therefore, it can be concluded that ε_i is decreasing function with respect to γ_i .

Appendix B

Proof of proposition 3.2.2

The first partial derivative of ε_i with R_i is given as

$$\frac{\partial}{\partial R_i} Q(\Xi(\gamma_i, R_i)) = -\frac{1}{\sqrt{2\pi}} e^{-\frac{1}{2}\Xi^2(\gamma_i, R_i)} \frac{\partial \Xi(\gamma_i, R_i)}{\partial R_i}, \quad (\text{B.1})$$

where

$$\frac{\partial \Xi(\gamma_i, R_i)}{\partial R_i} = -\frac{2}{\log_2 e \sqrt{2 \left(1 - \frac{1}{(1+\gamma_i)^2}\right)} / N} = -\Theta(\gamma_i). \quad (\text{B.2})$$

Then, $\frac{\partial}{\partial R_i} Q(\Xi(\gamma_i, R_i))$ in (B.1) can be expressed as

$$\frac{\partial}{\partial R_i} Q(\Xi(\gamma_i, R_i)) = \frac{1}{\sqrt{2\pi}} e^{-\frac{1}{2}\Xi^2(\gamma_i, R_i)} \Theta(\gamma_i). \quad (\text{B.3})$$

Since $\Theta(\gamma_i) \geq 0$, $\frac{\partial}{\partial R_i} Q(\Xi(\gamma_i, R_i)) \geq 0$. It can be concluded that ε_i is an increasing function with respect to R_i .

Appendix C

Proof of Lemma 3.2.4

To determine the optimal value of R_1 which maximizes \bar{T} , we examine the monotonicity and concavity of \bar{T} with respect to R_1 . The first and second derivatives of \bar{T} are examined as below.

Following (3.2), the first derivative of \bar{T} is given by

$$\begin{aligned} \frac{\partial \bar{T}}{\partial R_1} = & 1 - Q(\Xi(\gamma_{11}, R_1)) - R_1 \frac{\partial}{\partial R_1} Q(\Xi(\gamma_{11}, R_1)) \\ & - R_2 (1 - Q(\Xi(\gamma_{22}, R_2))) \frac{\partial}{\partial R_1} Q(\Xi(\gamma_{21}, R_1)). \end{aligned} \tag{C.1}$$

By substituting (B.3) into (C.1), the first derivative of \bar{T} with respect to R_1 is given by

$$\begin{aligned} \frac{\partial \bar{T}}{\partial R_1} = & 1 - Q(\Xi(\gamma_{11}, R_1)) - R_1 \frac{1}{\sqrt{2\pi}} \Theta(\gamma_{11}) e^{-\frac{1}{2}\Xi^2(\gamma_{11}, R_1)} \\ & - R_2 (1 - Q(\Xi(\gamma_{22}, R_2))) \frac{1}{\sqrt{2\pi}} \Theta(\gamma_{21}) e^{-\frac{1}{2}\Xi^2(\gamma_{21}, R_1)}. \end{aligned} \tag{C.2}$$

Since the value of (C.2) is not always positive or negative, \bar{T} is not an increasing

or decreasing function with respect to R_1 . Next, we examine the monotonicity of \bar{T} with respect to R_1 . Following (C.2), the second derivative of \bar{T} with respect to R_1 is given by

$$\begin{aligned} \frac{\partial^2 \bar{T}}{\partial R_1^2} &= -\frac{\partial}{\partial R_1} Q(\Xi(\gamma_{11}, R_1)) - \frac{1}{\sqrt{2\pi}} \Theta(\gamma_{11}) e^{-\frac{1}{2}\Xi^2(\gamma_{11}, R_1)} \\ &\quad - R_1 \frac{1}{\sqrt{2\pi}} \Theta(\gamma_{11}) \frac{\partial}{\partial R_1} e^{-\frac{1}{2}\Xi^2(\gamma_{11}, R_1)} \\ &\quad - R_2 (1 - Q(\Xi(\gamma_{22}, R_2))) \frac{1}{\sqrt{2\pi}} \Theta(\gamma_{21}) \frac{\partial}{\partial R_1} e^{-\frac{1}{2}\Xi^2(\gamma_{21}, R_1)}. \end{aligned} \quad (\text{C.3})$$

Using (B.2) and (B.3), (C.3) is presented as

$$\begin{aligned} \frac{\partial^2 \bar{T}}{\partial R_1^2} &= -\frac{2}{\sqrt{2\pi}} \Theta(\gamma_{11}) e^{-\frac{1}{2}\Xi^2(\gamma_{11}, R_1)} - R_1 \frac{1}{\sqrt{2\pi}} \Theta^2(\gamma_{11}) \Xi(\gamma_{22}, R_2) e^{-\frac{1}{2}\Xi^2(\gamma_{11}, R_1)} \\ &\quad - R_2 (1 - Q(\Xi(\gamma_{22}, R_2))) \frac{1}{\sqrt{2\pi}} \Theta^2(\gamma_{22}) \Xi(\gamma_{22}, R_2) e^{-\frac{1}{2}\Xi^2(\gamma_{22}, R_1)}. \end{aligned} \quad (\text{C.4})$$

Since $\Xi(\gamma_i, R_i) \geq 0$ and $\Theta(\gamma_i) \geq 0$, then $\frac{\partial^2 \bar{T}}{\partial R_1^2} \leq 0$. We can conclude that \bar{T} is the concave function with respect to R_1 . Therefore, the optimal R_1 can be derived by solving $\frac{\partial \bar{T}}{\partial R_2} = 0$.

Appendix D

Proof of Lemma 3.2.5

To find out the existence of the optimal transmission rate R_2 that maximizes \bar{T} , the monotonicity and concavity are examined by deriving the first and second derivatives of \bar{T} with respect to R_2 , presented as following.

From (3.2), the first derivative of \bar{T} with respect to R_2 is given by

$$\frac{\partial \bar{T}}{\partial R_2} = \left(1 - Q(\Xi(\gamma_{22}, R_2)) - R_2 \frac{\partial}{\partial R_2} Q(\Xi(\gamma_{22}, R_2)) \right) (1 - Q(\Xi(\gamma_{21}, R_1))). \quad (\text{D.1})$$

By substituting (C.2) into (D.1), we have

$$\frac{\partial \bar{T}}{\partial R_2} = \left(1 - Q(\Xi(\gamma_{22}, R_2)) - R_2 \frac{1}{\sqrt{2\pi}} (\gamma_{22}) e^{-\frac{1}{2}\Xi^2(\gamma_{22}, R_2)} \right) (1 - Q(\Xi(\gamma_{21}, R_1))). \quad (\text{D.2})$$

Since the value $\frac{\partial \bar{T}}{\partial R_2}$ is not always positive or negative, \bar{T} is not an increasing or decreasing function with respect to R_2 . Then, we examine the second derivative of

\bar{T} with respect to R_2 . From (D.2), we have

$$\begin{aligned} \frac{\partial^2 \bar{T}}{\partial R_2^2} = & \left(-\frac{\partial}{\partial R_2} Q(\Xi(\gamma_{22}, R_2)) - \frac{1}{\sqrt{2\pi}} \Theta(\gamma_{22}) e^{-\frac{1}{2}\Xi^2(\gamma_{22}, R_2)} \right. \\ & \left. - R_2 \frac{1}{\sqrt{2\pi}} \Theta(\gamma_{22}) \frac{\partial}{\partial R_2} e^{-\frac{1}{2}\Xi^2(\gamma_{22}, R_2)} \right) (1 - Q(\Xi(\gamma_{21}, R_1))). \end{aligned} \quad (\text{D.3})$$

By substituting (B.2) and (B.3) into (D.3), we have

$$\begin{aligned} \frac{\partial^2 \bar{T}}{\partial R_2^2} = & \left(-\frac{2}{\sqrt{2\pi}} \Theta(\gamma_{22}) e^{-\frac{1}{2}\Xi^2(\gamma_{22}, R_2)} - R_2 \frac{1}{\sqrt{2\pi}} \Theta^2(\gamma_{22}) \Xi(\gamma_{21}, R_1) e^{-\frac{1}{2}\Xi^2(\gamma_{22}, R_2)} \right) \\ & \times (1 - Q(\Xi(\gamma_{21}, R_1))). \end{aligned} \quad (\text{D.4})$$

Since $\Xi(\gamma_i, R_i) \geq 0$ and $\Theta(\gamma_i) \geq 0$, $\frac{\partial^2 \bar{T}}{\partial R_2^2} \leq 0$. Therefore, the sum throughput \bar{T} is the concave function with respect to R_2 . The optimal R_2 can be obtained by solving $\frac{\partial \bar{T}}{\partial R_2} = 0$.

Bibliography

- [1] L. U. Khan, “Visible light communication: Applications, architecture, standardization and research challenges,” *Digital Communications and Networks*, vol. 3, no. 2, pp. 78–88, May 2017.
- [2] S. Dimitrov and H. Haas, *Principles of LED light communications: towards networked Li-Fi*. Cambridge University Press, Mar. 2015.
- [3] L. E. M. Matheus, A. B. Vieira, L. F. Vieira, M. A. Vieira, and O. Gnawali, “Visible light communication: concepts, applications and challenges,” *IEEE Commun. Surv. Tutor.*, vol. 21, no. 4, pp. 3204–3237, Apr. 2019.
- [4] O. N. Yilmaz, Y.-P. E. Wang, N. A. Johansson, N. Brahmi, S. A. Ashraf, and J. Sachs, “Analysis of ultra-reliable and low-latency 5g communication for a factory automation use case,” in *Proc. IEEE Int. Conf. Commun. Workshop (ICCW)*. IEEE, Jun. 2015, pp. 1190–1195.
- [5] G. Durisi, T. Koch, and P. Popovski, “Toward massive, ultrareliable, and low-latency wireless communication with short packets,” *Proc. IEEE*, vol. 104, no. 9, pp. 1711–1726, Sept. 2016.

- [6] Sutton *et al.*, “Enabling technologies for ultra-reliable and low latency communications: From phy and mac layer perspectives,” *IEEE Commun. Surv. Tutor.*, vol. 21, no. 3, pp. 2488–2524, 3rd Quart. 2019.
- [7] Y. Polyanskiy, H. V. Poor, and S. Verdú, “Channel coding rate in the finite blocklength regime,” *IEEE Trans. Inf. Theory*, vol. 56, no. 5, pp. 2307–2359, May 2010.
- [8] W. Yang, G. Durisi, T. Koch, and Y. Polyanskiy, “Quasi-static multiple-antenna fading channels at finite blocklength,” *IEEE Trans. Inf. Theory*, vol. 60, no. 7, pp. 4232–4265, Jul. 2014.
- [9] S. I. Bross, A. Lapidoth, and S. Tinguely, “Broadcasting correlated gaussians,” *IEEE Trans. Inf. Theory*, vol. 56, no. 7, pp. 3057–3068, Jul. 2010.
- [10] Shirvanimoghaddam *et al.*, “Short block-length codes for ultra-reliable low latency communications,” *IEEE Commun. Mag.*, vol. 57, no. 2, pp. 130–137, Feb. 2019.
- [11] A. Lapidoth and S. Tinguely, “Sending a bivariate gaussian over a gaussian mac,” *IEEE Trans. Inf. Theory*, vol. 56, no. 6, pp. 2714–2752, Jun. 2010.
- [12] A. Karimi, K. I. Pedersen, N. H. Mahmood, G. Pocovi, and P. Mogensen, “Efficient low complexity packet scheduling algorithm for mixed urllc and embb traffic in 5g,” in *Proc. IEEE 89th Veh. Technol. Conf. (VTC2019-Spring)*. IEEE, Kuala Lumpur, Malaysia, Apr. 2019, pp. 1–6.
- [13] H.-M. Wang, Q. Yang, Z. Ding, and H. V. Poor, “Secure short-packet communications for mission-critical iot applications,” *IEEE Trans. Wirel. Commun.*, vol. 18, no. 5, pp. 2565–2578, May, 2019.

- [14] B. Makki, T. Svensson, and M. Zorzi, “Finite block-length analysis of spectrum sharing networks using rate adaptation,” *IEEE Transactions on Communications*, vol. 63, no. 8, pp. 2823–2835, Aug. 2015.
- [15] W. Yang, G. Caire, G. Durisi, and Y. Polyanskiy, “Optimum power control at finite blocklength,” *IEEE Trans. Inf. Theory*, vol. 61, no. 9, pp. 4598–4615, Sept. 2015.
- [16] S. Xu, T.-H. Chang, S.-C. Lin, C. Shen, and G. Zhu, “Energy-efficient packet scheduling with finite blocklength codes: Convexity analysis and efficient algorithms,” *IEEE Trans. Wirel. Commun.*, vol. 15, no. 8, pp. 5527–5540, Aug. 2016.
- [17] S. Dimitrov, S. Sinanovic, and H. Haas, “Clipping noise in ofdm-based optical wireless communication systems,” *IEEE Trans. Commun.*, vol. 60, no. 4, pp. 1072–1081, Mar. 2012.
- [18] Z. Wang, Z. Lin, T. Lv, and W. Ni, “Energy-efficient resource allocation in massive mimo-noma networks with wireless power transfer: A distributed admm approach,” *IEEE Internet Things J.*, vol. 8, no. 18, pp. 14 232–14 247, Sept. 2021.
- [19] Z. Ding, F. Adachi, and H. V. Poor, “The application of mimo to non-orthogonal multiple access,” *IEEE Trans. Wirel. Commun.*, vol. 15, no. 1, pp. 537–552, Jan. 2015.
- [20] J. Men and J. Ge, “Non-orthogonal multiple access for multiple-antenna relaying networks,” *IEEE Commun. Lett.*, vol. 19, no. 10, pp. 1686–1689, Oct. 2015.

- [21] Y. Song, W. Yang, Z. Xiang, N. Sha, H. Wang, and Y. Yang, “An analysis on secure millimeter wave noma communications in cognitive radio networks,” *IEEE Access*, vol. 8, pp. 78 965–78 978, 2020.
- [22] G. N. Tran and S. Kim, “Performance analysis of short packets in noma vlc systems,” *IEEE Access*, vol. 10, pp. 6505–6517, Jan. 2022.
- [23] H. Marshoud, V. M. Kapinas, G. K. Karagiannidis, and S. Muhaidat, “Non-orthogonal multiple access for visible light communications,” *IEEE Photonics Technol. Lett.*, vol. 28, no. 1, pp. 51–54, Jan. 2016.
- [24] L. Yin, W. O. Popoola, X. Wu, and H. Haas, “Performance evaluation of non-orthogonal multiple access in visible light communication,” *IEEE Trans. Commun.*, vol. 64, no. 12, pp. 5162–5175, Sept. 2016.
- [25] H. Marshoud, P. C. Sofotasios, S. Muhaidat, G. K. Karagiannidis, and B. S. Sharif, “On the performance of visible light communication systems with non-orthogonal multiple access,” *IEEE Trans. Wirel. Commun.*, vol. 16, no. 10, pp. 6350–6364, Oct. 2017.
- [26] C. Chen, W.-D. Zhong, H. Yang, and P. Du, “On the performance of mimo-noma-based visible light communication systems,” *IEEE Photonics Technol. Lett.*, vol. 30, no. 4, pp. 307–310, Feb. 2017.
- [27] Y. Yu, H. Chen, Y. Li, Z. Ding, and B. Vucetic, “On the performance of non-orthogonal multiple access in short-packet communications,” *IEEE Commun. Lett.*, vol. 22, no. 3, pp. 590–593, Mar. 2017.
- [28] S. Han, X. Xu, Z. Liu, P. Xiao, K. Moessner, X. Tao, and P. Zhang, “Energy-efficient short packet communications for uplink noma-based massive mtc net-

- works,” *IEEE Trans. Veh. Technol.*, vol. 68, no. 12, pp. 12 066–12 078, Oct. 2019.
- [29] M. B. Janjua, D. B. da Costa, and H. Arslan, “User pairing and power allocation strategies for 3d vlc-noma systems,” *IEEE Wirel. Commun. Lett.*, vol. 9, no. 6, pp. 866–870, Jun. 2020.
- [30] C. Du *et al.*, “Secure transmission for downlink noma visible light communication networks,” *IEEE Access*, vol. 7, pp. 65 332–65 341, 2019.
- [31] G. N. Tran and S. Kim, “Performance evaluation of short packet communications in noma vlc systems with imperfect csi,” *IEEE Access*, vol. 10, pp. 49 871–49 793, May 2022.
- [32] W. M. D.D. Wackerly and R. Scheaffer, *Mathematical statistics with applications*. Duxbury Press, 1996.
- [33] P. F. Z. Ding, Z. Yang and H. V. Poor, “On the performance of non-orthogonal multiple access in 5g systems with randomly deployed users,” *IEEE Signal Process. Lett.*, vol. 21, no. 12, pp. 1501—1505, 2014.
- [34] M. Abramowitz and E. I. A. Stegun, *Handbook of mathematical functions with formulas, graphs, and mathematical tables*. tenth printing ed. Washington, DC, USA: U.S. Government Printing Office, 1972.
- [35] M. Shirvanimoghaddam *et al.*, “Short block-length codes for ultra-reliable low latency communications,” *IEEE Commun. Mag.*, vol. 57, no. 2, pp. 1—8, Dec. 2018.